Fitoterapia 149 (2021) 104811

Contents lists available at ScienceDirect

Fitoterapia

journal homepage: www.elsevier.com/locate/fitote

Chlorinated bianthrones from the cyanolichen *Nephroma laevigatum*

Aurélie Lagarde [a], Lengo Mambu [a], Phuong-Y. Mai [a], Yves Champavier [b], Jean-Luc Stigliani [c], Mehdi A. Beniddir [d,*], Marion Millot [a,*]

[a] Departement de Pharmacognosie, Faculté de Pharmacie, Université de Limoges, 2 rue du Dr Marcland, 87025 Limoges Cedex, France
[b] Plateforme BISCEm, Université de Limoges, 2 Rue du Pr Descottes, 87025 Limoges Cedex, France
[c] Laboratoire de Chimie de Coordination, UPR CNRS 8241, Université de Toulouse UPS, France
[d] Équipe "Chimie des Substances Naturelles", Université Paris-Saclay, CNRS, BioCIS, 5, rue J.-B. Clément, 92290 Châtenay-Malabry, France

ARTICLE INFO

Keywords:
Bianthrones
Dereplication
NMR calculations
Lichens
Nephroma

ABSTRACT

While depsidones, depsides or dibenzofuran-like compounds dominate the chemical composition of lichens, the cyanolichen *Nephroma laevigatum* affords a diversity of quinoid pigments represented by chlorinated anthraquinones derived from emodin and new bianthrones resulting from the homo- or heterodimerization of monomers. Bianthrones were pointed out from the dichloromethane extract by MS/MS-based molecular networking, then isolated and characterized on the basis of extensive spectroscopic analyzes and GIAO NMR shift calculation followed by CP3 analyzes.

1. Introduction

Nephroma laevigatum Ach. is a lichenized Ascomycota belonging to the Nephromataceae family (Peltigerales order). It is a foliose lichen with a cyanobiont (Nostoc) as photosynthesizing partner [1]. The first phytochemical investigation of this lichen was conducted by Bentz et al., who isolated five anthraquinones (emodin (**1**) and chlorinated derivatives) from a Swedish specimen [2]. A few years later, a North American specimen was studied by Cohen et al. They described the presence of chlorinated anthraquinones [3]. Beside these hydroxyanthraquinone pigments, *N. laevigatum* is known for its hopane triterpenoids. Nephrin is the only triterpenoid reported and isolated from this species [4]. A more recent study revealed the presence of mycosporine hydroxyglutamicol from an aqueous-methanolic extract [5]. Mycosporine-like amino-acids were commonly associated with cyanolichen metabolism and are involved in photoprotection of the photobiont. A recent study on *Nephroma laevigatum* reports the endolichenic fungi growing inside this lichen thallus [6]. This lichen shows a rather low diversity of endolichenic fungi in comparison to other genera with a predominance of *Nemania* species. In an extensive research conduct on the Genus *Nephroma*, a French specimen was collected in a humid forest to deeply explore the anthraquinone content. Thus dichloromethane extract, particularly rich in quinoid pigments was profiled by LC-MS/MS and then purified in order to isolate anthraquinones and bianthrones. This phytochemical investigation allowed the identification of two new diastereoisomeric pairs of chlorinated bianthrones (**5**–**6**). Due do their chemical instability, few bianthrones with a C10–C10′ linkage, have been tested for their biological activity. Chrysophanol bianthrones and emodin-physcion bianthrone have shown significant cytotoxicity activity against KB, HL-60 and A-459 cell lines [7,8]. Anti-plasmodial activities have been described for some prenylated bianthrones [9]. Finally, the ability of such compound to generate singlet oxygen upon exposure to light contributes to a photodynamic potential toward bacteria and cancer cells [10].

2. Results and discussion

2.1. UV- and MS-based dereplication and isolation

Extraction of the dried lichen thallus with dichloromethane by maceration at room temperature gave a brown extract enriched in quinoid pigments easily visualized on TLC. Fractionation of the extract by silica gel chromatography yielded several fractions. These fractions were analyzed by HPLC-DAD and showed two main groups of compounds with distinct UV absorptions. The first group displays a UV spectrum with four main bands at 210–232; 271–280; 308–310 and 420–490 nm characteristic of anthraquinones [11]. The second group displays a different UV spectrum with two main bands at 278–280 and

* Corresponding authors.
E-mail addresses: lengo.mambu@unilim.fr (L. Mambu), yves.champavier@unilim.fr (Y. Champavier), jean-luc.stigliani@lcc-toulouse.fr (J.-L. Stigliani), mehdi.beniddir@universite-paris-saclay.fr (M.A. Beniddir), marion.millot@unilim.fr (M. Millot).

https://doi.org/10.1016/j.fitote.2020.104811
Received 1 October 2020; Received in revised form 8 December 2020; Accepted 9 December 2020
Available online 7 January 2021

358–360 nm strongly suggesting the presence of bianthronic compounds [12].

In an attempt to map the chemical diversity of the dichloromethane extract, the LC-MS/MS data were processed using the feature-based molecular networking workflow [13] and subsequently dereplicated against the Lichen Database (LDB) [14], hosted by GNPS [15]. The molecular networking-based dereplication process afforded only two hits (emodine and 7-*O*-methylfragilin). These results reveal the lack of lichen compounds references in MS/MS databases and the high potential for new compounds discovery in *N. laevigatum*. The quest for tackling the issue of molecular networking annotation has fueled a number of creative and successful endeavors from the community, including our group [16–19]. Hence, as part of our continuous interest in the discovery of new chlorinated quinoids pigments, the molecular network was color-coded (Fig. 1 and S1 in supporting information for the whole molecular network) based on the halogenation pattern (1 × Cl, 2 × Cl) of the fragmented parent masses. This annotation revealed that there were over 50 metabolites possessing at least a single chlorine in their chemical structure. Consequently, we focused isolation efforts on molecules that exhibited the aforementioned UV absorptions in addition to their chlorination pattern. Using these UV- and MS-guided isolation approaches, we were able to isolate and characterize eight compounds: four anthraquinones (emodin, 7-chloro-emodin, 7-chloro-1-*O*-methyl-emodin and 1-*O*-methylfragilin (**1**–**4**)) [2,3], two new homobianthrones (diasteroisomers **5a** and **5b**) and two new heterobianthrones (diasteroisomers **6a** and **6b**).

2.2. Structural elucidation

Bianthrones isomers were isolated as pale-yellow amorphous powder. Compounds **5a** and **5b**, shared the same molecular formula, $C_{30}H_{20}O_8Cl_2$, deduced from its HR-ESI-MS spectra which showed a pseudo-molecular ion $[M\text{-}H]^-$ at *m/z* 577.0488 indicating a degree of unsaturation of twenty. Moreover, the intensity of peaks observed in the isotopic cluster is consistent with the presence of two chlorine atoms in the molecule. With the same molecular formula but different retention times in HPLC, **5a** and **5b** were suggested to be diastereoisomers. The ^{13}C NMR spectrum indicated 15 carbon signals including one carbonyl group, nine quaternary carbons, four methines and one methyl groups. In the ^1H NMR spectrum of compound **5a** (Table 1), three broad singlet at δ_H 12.49, 11.59 and 11.55 ppm indicated the presence of hydroxyl groups, three aromatic protons at δ_H 6.73, 6.27 and 6.23 ppm, one methine group at δ_H 4.54 ppm and one methyl group at δ_H 2.25 ppm. The molecular formula, ^1H and ^{13}C NMR data (Table 1) suggest that compounds **5a** and **5b** result from the dimerization of 7-chloroemodin (**2**) to form a homobianthrone. In comparison with isolated anthraquinones, the disappearance of one carbonyl group as well as the appearance of a methine carbon at δ_C 53.5 ppm correlated with the proton at δ_H 4.54 ppm suggest a reduction of the carbonyl at C-10 in favor of the linkage of the two monomer moieties at C-10 and C-10′. Thanks to HSQC NMR experiment, aromatic protons at 6.73, 6.27 and 6.23 ppm were correlated to carbons at δ_C 115.2, 107.5 and 120.2 respectively. Information obtained from the HMBC spectrum allowed to establish without any ambiguity the structure of compound **5a**. The methyl protons at 2.25 ppm were correlated with carbons at δ_C 115.2 (C-2), 120.2 (C-4) and 145.7 (C-3) while H-2 at 6.73 was correlated with carbons at δ_C 139.4 (C-9a), 120.3 (C-4) and 20.4 (CH_3-3). Connectivities of OH-8 at 12.49 ppm with carbon at δ_C 104.9 (C-7) and 108.3 (C-8a) confirmed the position of chlorine atom at C-7 while H-5 was in correlation with C-8a. The hydroxyl proton (OH-8) can be stabilized by hydrogen bonding with the ketone, unlike the hydroxyl proton in position 6 and 6′, which appear in the spectrum as a broad singlet. Notably, HMBC correlations of the methine proton (*H*−10) at 4.54 ppm with carbons at δ_C 53.5 (C-10′), 112.4 (C-10a), 120.2 (C-4), 139.4 (C-9a) and 139.5 (C-4a) and were helpful for the attribution of quaternary carbons. It also comforts the linkage of the two monomer units at C-10 and C-10′.

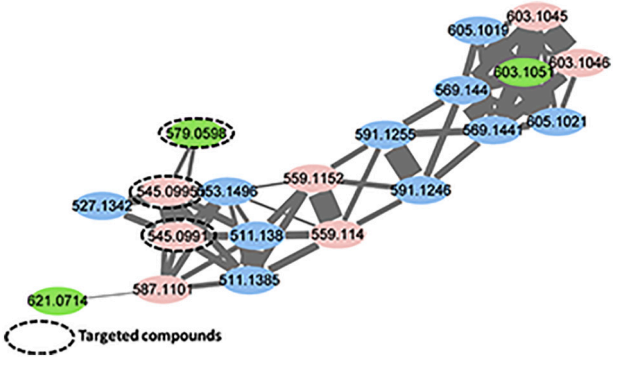

Fig. 1. Molecular family containing the new targeted chlorinated bianthrones (color-coding of the halogenation pattern is as follows: red = Cl, green = 2 × Cl).

The presence of two asymmetric carbons at C-10 and C-10′ easily explains the coexistence of two diastereoisomers. It is noteworthy that among the aromatic protons, the signal at δ_H 6.73 ppm is well defined while the other two signals at δ_H 6.27 and 6.23 ppm are broad singlets. This could be explained by the chemical environment of these protons. The aromatic proton at δ_H 6.73 ppm attached to the C-2 carbon is stabilized by the involvement of the hydroxyl group at C-1 in a hydrogen bond with the carbonyl and by the presence of the methyl group (C-3). Conversely, the protons H-4 and H-5 were influenced by the relatively unstable methine proton (C-10) and the steric hindrance and appeared as broad singlets.

For the stereoisomer **5b**, the ^1H NMR spectrum showed slightly different chemical shifts. Protons H-2, H-4, OH-6 and CH_3-3 were shielded while protons H-5, OH-6 and OH-8 were deshielded. Due to the degradation of compound in solution during NMR acquisition, ^{13}C NMR data could not be acquired.

With a molecular formula of $C_{30}H_{21}O_8Cl$ deduced from its HR-ESI-MS at *m/z* 543.0867 $[M\text{-}H]^-$, and non-overlapped ^{13}C NMR signals (Table 1), compounds **6a** and **6b** are supposed to be heterobianthrones. Considering the loss of one chlorine replaced by an additional proton at δ_H 6.20 (d, 1.9 Hz, H-7′), these asymmetric compounds were identified as diastereoisomeric pairs of 7-chloroemodin-emodin heterodimers. The ^1H NMR spectrum of compound **6a** showed six singlets between 10.80 and 12.53 ppm, seven aromatic protons, two methine protons and two methyl groups. Among the aromatic protons, as observed for homobianthrones, three protons are well defined (H-7′, H-2 and H-2′) while four are broad signals (H-4, H-4′, H-5 and H-5′). The ^{13}C RMN spectrum of compound **6a** showed similarities with that of compound **5a** and **5b** except for C-6′, C-7′ and C-8′ carbons. C-7′ was shielded by +3.4 ppm while C-6′ and C-8′ were deshielded by +5.8 ppm and + 5.7 ppm, respectively. These variations of chemical shifts reflect the loss of the chlorine atom on the C-7′ position. The correlations observed in the HMBC spectrum for the hydroxyl protons confirm the carbon assignments. The hydroxyl proton at δ_H 12.60 ppm attached to the C8 carbon has a well-defined signal due to its stabilization by the ketone group at C-9 and the chlorine at C-7. This hydroxyl proton showed correlations with C-7, C-8 and C-8a.

In the other moiety, the hydroxyl proton at δ_H 11.92 attached to the C-8′ carbon is less shielded due to the absence of the chlorine atom and showed correlations with C-7′, C-8′ and C-8a′. The HMBC correlations of the hydroxyl proton at δ_H 11.52 with C-1, C-9a and C-2 justify its position on carbon C-1. The hydroxyl group at δ_H 10.75 ppm showed correlations with C-5′, C-6′ and C-7′ whereas the hydroxyl group at δ_H 11.50 (OH-6) next to the chlorine is shielded and without any correlation. As in the homobianthrones (**5a** and **5b**), the hydroxyl group at C-6 displayed a broad signal without clear correlations. Nevertheless, a small correlation is observed with C-5. The correlation of the methine proton at δ_H 4.50 ppm with C-4a, C-8a and C-10a allowed to confirm the

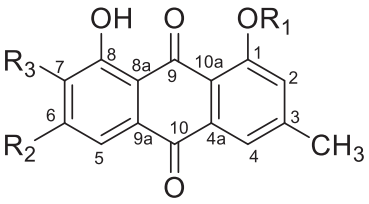

1 $R_1 = R_2 = R_3 = H$
2 $R_1 = R_2 = H$, $R_3 = Cl$
3 $R_1 = CH_3$, $R_2 = H$, $R_3 = Cl$
4 $R_1 = R_2 = CH_3$, $R_3 = Cl$

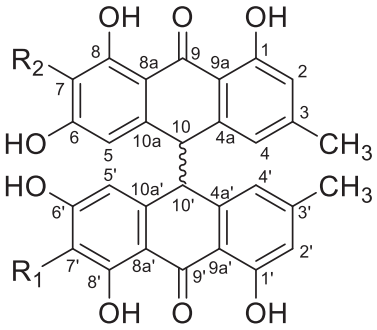

5 $R_1 = R_2 = Cl$
6 $R_1 = H$, $R_2 = Cl$

chemical shift of the central quaternary carbons.

For compound **6b**, the main difference is observed in the ^1H NMR spectrum compared to **6a** with the deshielding of the aromatic protons H-4′. This difference is supposed to be the consequence of a modification of the spatial configuration.

Similar chlorinated bianthrones have already been isolated from the lichens *Heterodermia obscurata* and *Anaptychia obscurata* and are called flavoobscurin A and B [20,21]. These new compounds, identified for the first time in the lichen *N. laevigatum* were named nephrolaevigatin A and nephrolaevigatin B (**5a** and **5b**) for the homobianthrones and nephrolaevigatin C and nephrolaevigatin D (**6a** and **6b**) for the heterobianthrones.

2.3. Relative configuration assignment

Stereochemistry of bianthrones remains difficult to establish due to the *meso*, racemic and axis rotation phenomena. ^1H—^1H *J* coupling constant magnitudes of H10-H10′ as well as NOESY correlations spectra are often cited in literature but are not sufficient to establish properly the relative configurations of these compounds. Even the specific optical rotation is uncertain, due to the possible impurity of *meso* compounds or 1:1 ratio for enantiomers (scalemic mixture). Consequently, NMR chemical shifts analysis and computational approaches are emerging as alternatives strategies to tackle this issue [22]. In the ^1H NMR spectrum of homobianthrones nephrolaevigatin A and nephrolaevigatin B (**5a** and **5b**), H-10 and H-10′ protons appear as a singlet without coupling constant due to the symmetry of the molecule. Thus, chemical shifts are the only informative data. Based on computational and experimental results obtained by Ji et al. [23], the NMR data of compounds **5** and **6** provided interesting information. Comparison of ^1H NMR data of homobianthrones **5a** and **5b** with *cis* and *trans* emodin bianthrones, suggests that **5a** is a *trans* isomer and **5b** is a *cis* isomer. Indeed, the isomer **5b** possesses higher frequency ^1H NMR signals for rings A and A′ (H-2, CH_3-3 and H-4) and lower-frequencies for rings B and B′ (H-5) (Fig. S2). Thus, according to optical rotation values, we concluded that **5a** is a racemate and **5b** is a *meso* form.

An inspection of ^1H NMR data of the heterobianthrones **6a** and **6b**, revealed slight differences in ^1H—^1H *J* coupling constant magnitudes of H-10 and H-10′. According to Aly et al., a coupling constant of 2.0 Hz between H-10 and H-10′ required that these protons have a *cis* relationship [24]. A coupling constant of 4.7 Hz is observed for compound **6a** (Table 1), suggesting that **6a** possesses a C-10 – C10′ junction in a *trans* configuration. In compound **6b**, a coupling constant of 3.0 Hz is in favor of a *cis* isomer.

In order to confirm the aforementioned assignments, Gauge-Independent Atomic Orbital (GIAO) NMR ^1H and ^{13}C chemical shifts calculations were performed on diastereoisomers **5** and **6**. The sigma C-10 – C10′ bond enables the two anthraquinone rings to rotate to each other; hence, heterobianthrones may take different conformations. A Conformational analysis performed around this bond showed that each structure can exhibit, by regard to the bond, two face to face stacked forms (*gauche* conformations) and an *anti*-one where ring systems are not stacked (Fig. 2 and S3). Quantum chemical geometry optimizations and vibrational frequency calculations indicated that the *gauche* forms are clearly more stables than the *anti*-ones. This observation has already been reported by Ji *et al* [23].

The evaluation of the Boltzmann populations of each conformer of **5** and **6** showed that the *anti* conformer is negligible comparing to two *gauche* ones (Table 2). In addition, one can notice that for the (10*R*, 10′*R*)-**5** and **6** enantiomers, one of the two *gauche* conformers is more stable about 2.5 $kJ.mol^{-1}$, than the second one: the difference is due to the steric hindrance induced by the proximity of the 3′-CH_3 and the 7-Cl found in the stacked gauche-1 conformers (Fig. 2).

In the CP3 approach, the difference between the experimental and the *ab initio* calculated ^{13}C and ^1H NMR scaled chemical shifts is computed. The probability that experimental and theoretical data match is then calculated [25].

For compounds **5** and **6**, two sets of resonance signals were obtained, to which two diastereoisomers must be assigned. CP3 parameters were then determined for all possible pairs of diastereoisomers of the *gauche* conformers of **5** and **6**. Unfortunately, we were unable to exploit the ^1H NMR chemical shifts, because they were too close for both compounds **5a** and **5b**. Furthermore, ^{13}C NMR data were not available for compound **5b**. Therefore, we give only results for the isomers of compounds **6a** and **6b**.

The CP3 results allowed to attribute the (10*R**, 10′*S**) relative configuration isomer for compound **6a** and the (10*R**, 10′*R**) one for compound **6b** (Table 3). In addition, the results are in favor of the *gauche*-2 conformation for **6b** which is indeed the most stable conformer (Table 2). In the case of **6a**, CP3 values (Table 3) are very close for the (10*R*, 10′*S*) *gauche*-1 and (10*R*, 10′*S*) *gauche*-2 conformers: 0.81 and 0.73 respectively. In fact, these two conformers exhibit a similar energy and each contributes to the Boltzmann population for about 50% (Table 2). At last, according to optical rotation value we concluded that **6b** occurs as a racemate.

It is important to note that the instability of bianthrones in solution have been observed during the purification process, which greatly hampered identification. Notable changes were observed i) in the physical state with color changes from pale-yellow to red-dark or green-dark ii) by HPLC-DAD with the apparition of additional peaks iii) during the NMR acquisition time in solvents such as acetone or dimethylsulfoxide with a decrease in the intensity of the main compound in favor of the formation of secondary products corresponding to anthraquinone monomers (Supporting informations). Indeed, bianthrones are known to

Table 1
NMR spectroscopic data of **5a**, **b** and **6a**, **b** at 500 MHz (^{1}H) and 125 MHz (^{13}C) in DMSO-d_6.

	5a, b			**6a, b**		
	δ_C	δ_H, mult(*J* (Hz))	HMBC	δ_C	δ_H, mult(*J* (Hz))	HMBC
1	159.7			160.8		
2	115.2	6.73, s/ 6.71, s	C-4; C-9a; CH_3-3	116.2	6.67, s/ 6.71, s	C-1; C-4; C-9a; CH_3-3
3	145.7			146.8		
4	120.2	6.23[a], s/ 6.19[a], s		121.3	6.15[a], s/ 6.17[a], s	
5	107.5	6.27[a], s/ 6.33[a], s	C-8a	109.1	6.12[a], s/ 6.09[a], s	
6	158.6			158.6/ 158.9		
7	104.9			105.8		
8	157.8			159.6		
9	188.3			189.4		
10	53.5	4.54, s	C4a; C9a; C10a	55.0	4.50, d (4.7)/4.50, d(3.0)	C-4; C-4a; C-8a; C-10a
4a	139.5			140.0/ 140.5		
8a	108.3			109.2		
9a	139.4			113.6		
10a	112.4			142.5/ 140.8		
OH-1	–	11.59, s/ 11.50[a], s		–	11.52, s/ 11.60[a], s	C-1; C-2; C-9a
OH-6	–	11.55[a], s/ 11.61[a], s		–	11.50[a], s/ 11.49[a], s	
OH-8	–	12.49, s/ 12.58, s	C-7; C-8; C-8a	–	12.60, s/ 12.53, s	C-7; C-8; C-8a
CH_3-3	20.4	2.25, s	C-2; C-3; C-4	21.5	2.21, s/ 2.25, s	C-2; C-3; C-4
1′	159.7			160.8		
2′	115.2	6.73, s/ 6.71, s	C-4′; C-9a′; CH_3-3′	116.3	6.68, s/ 6.73, s	C-1′; C-4′; C-9a′; CH_3-3′
3′	145.7			146.2		
4′	120.2	6.23[a], s/ 6.19[a], s		121.2	6.40[a], s/ 6.31[a], s	
5′	107.5	6.27[a], s/ 6.33[a], s	C-8a′	108.6	6.25, d (2.0)/ 6.25[a], s	C-6′; C-8a′
6′	158.6			164.4		
7′	104.9			101.5/ 101.8	6.20, d (2.0)/6.19 d(1.9)	C-8a′
8′	157.8			163.5/ 163.7		
9′	188.3			189.4		
10′	53.5	4.54, s	C-4a′; C-9a′; C-10a′	54.7	4.56, d (4.7)/4.54, d(3.0)	C-4a′; C-4a; C-8a′; C-10a′
4a′	139.5			140.4/ 140.7		
8a′	108.3			109.6		
9a′	139.4			143.2		
10a′	112.4			113.8		
OH-1′	–	11.59, s/ 11.56[a], s		–	11.65, s/ 11.79, s	C-1′; C-2′; C-9a′
OH-6′	–	11.55[a], s/ 11.61[a], s		–	10.75[a], s/ 10.80[a], s	C-5′; C-6′; C-7′
OH-8′	–	12.49, s/ 12.58, s	C-7′; C-8′; C-8a′	–	11.92, s/ 11.86, s	C-7′; C-8′; C-8a′
CH_3-3′	20.4	2.25, s/ 2.22, s	C-2′; C-3′; C-4′	21.4	2.22, s/ 2.27, s	C-2′; C-3′; C-4′

[a] Broad signals.

reversibly change color in solution from bright yellow to dark green when subjected to heat (thermochromism) or light (photochromism) [26,27]. Similar changes were also observed when crystals of bianthrones were submitted to pressure [28]. Johnstones et al., assume that the color change observed here, from yellow to red or green, results from the coexistence of two forms (folded and twisted) [28]. The folded form is the more stable, but transition to the twisted form can be promoted either thermochemically or photochemically in solution. It has also been shown that the ability of the hydroxide ion to act as a one-electron reducing agent is low in aqueous media, but enhanced in aprotic solvents such as acetonitrile and dimethylsulfoxide (solvent used for the isolation and NMR analysis respectively) [29]. The first step in the reduction process is a fast and reversible polar-clustering reaction. This nucleophilic addition step results in a quinone-hydroxy complex followed by a slower electron-transfer step that produces the semi-quinone form [29,30]. LC-MS/MS analysis of the compound after degradation (color change from pale-yellow to red dark) showed the apparition of monomer ions as well as the formation of hypericine-like compounds (reduction of the C10–C10′ linkage) [30] (Fig. 3). Surprisingly, no degradation processes were reported in literature for flavoobscurin A and B or other related bianthrones after purification using a mixture of CH_2Cl_2 and MeOH or involving acetone.

Anthraquinones are widely biosynthesized in nature by higher plants (Liliaceae, Polygonaceae, Rhamnaceae and Cesalpinaceae), fungi or lichens [31]. Their biosynthesis implies the polyketide pathway [32]. The metabolism of halogenated compounds is restricted to fungi or lichenized fungi. In lichens, parietin is the most frequent anthraquinone biosynthesized by *Xanthoria* or *Caloplaca* species, but anthraquinones pigments are particularly prominent in the families of Nephromataceae, Physciaceae and Telochistaceae [2,21,33,34].

Bianthrones are more scarcely ever isolated. As demonstrated in this work, it could be explained by the difficulty to access to these compounds through purification process due to their instability and rapid degradation. Beside flavoobscurins isolated from the lichen *H. obscurata*, two chlorinated bianthrones, were isolated from the endophytic fungus *Penicillium* sp. (accession number HQ112180) [24] and from *Aspergillus alliaceus* [35]. Emodin bianthrones were isolated from *Polygonum multiflorum*. Prenylated bianthrones were isolated from higher plants, such as *Vismia laurentii*, *Psorospermum glaberrrium* [9,36] or fungus *Aspergillus wentii* [22].

3. Conclusion

These results highlight the chemical complexity of 10–10′ bianthrones. These biosynthetic intermediates between anthraquinones and naphtobianthrones can be abundant in lichens. The flexible connection between the two anthraquinones moieties gives rise to the existence of different isomers or conformers. Despite the difficulty for the chemist to isolate and properly identify bianthrones, they constitute interesting agents endowed with biological activities close to those of anthraquinones and naphtobianthrones.

4. Experimental section

4.1. General experimental procedures

^{1}H NMR and ^{13}C NMR spectra were acquired with a Bruker Avance III HD spectrometer at 500 and 125 MHz, respectively (Platform BISCEm Limoges, France). CD spectra were measured at 25 °C on a JASCO *J*-710 spectropolarimeter. High-resolution mass spectrometry (HRMS) measurements for exact mass determination were performed on a Micromass ZabspecTOF spectrometer for chemical ionization (Platform BISCEm, Limoges, France). Analytical HPLC was done on a Waters Alliance 2690 using a reversed-phase C_{18} Hibar® LiChrospher® 100 column (250 × 4 mm, 10 µm, Merck) and using a photodiode-array detector (Waters 996). Semi-preparative HPLC was performed using a HPLC Waters 600 (Controller, Pumpand Inline Degasser AF) on a Nucleodur® C_{18} HTec column (250 × 21 mm, 10 µm, Macherey- Nagel). HPLC conditions consisted of isocratic elution at a flow rate of 20 mL/min with 63% A/ 37% B for 30 min (A = 0.1% trifluoroacetic acid – acetonitrile; B = 0.1%

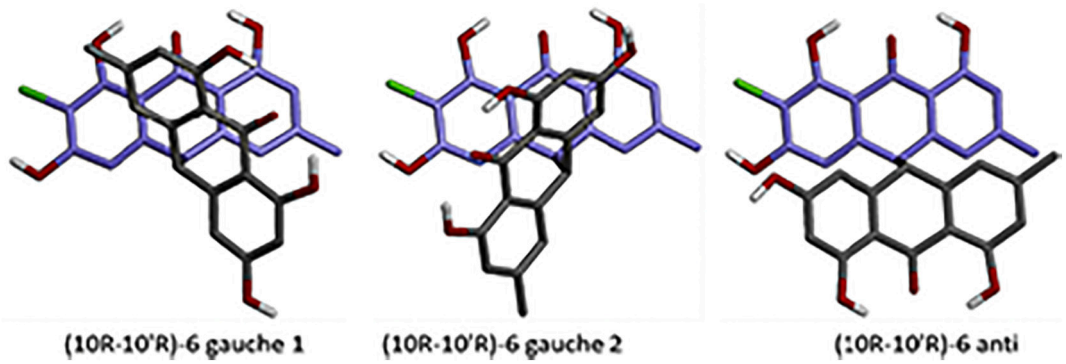

Fig. 2. Lowest-energy *gauche* and *anti* conformers of (10*R*-10′*R*) heterobianthrones **6**. For clarity, apolar hydrogens were omitted.

Table 2
The relative energy and the Boltzmann populations of conformers for bianthrones **5** and **6**.

Conformers	Relative Energy kJ.mol^{-1}	Boltzmann population
(10*R*,10′*R*)-**5***gauche* 1	2.61	0.25
(10*R*,10′*R*)-**5***gauche* 2	0.00	0.73
(10*R*,10′*R*)-**5***anti*	9.23	0.02
(10*R*,10′*S*)-**5***gauche* 1	0.00	0.50
(10*R*,10′*S*)-**5***gauche* 2	0.01	0.49
(10*R*,10′*S*)-**5***anti*	9.85	0.01
(10*R*,10′*R*)-**6***gauche* 1	2.58	0.26
(10*R*,10′*R*)-**6***gauche* 2	0.00	0.74
(10*R*,10′*R*)-**6***anti*	14.40	0.00
(10*R*,10′*S*)-**6***gauche* 1	0.18	0.48
(10*R*,10′*S*)-**6***gauche* 2	0.00	0.52
(10*R*,10′*S*)-**6***anti*	11.57	0.00

Table 3
Best CP3 values and related probabilities for the diastereoisomers (10*R*,10′*R*) and (10*R*,10′*S*) for compounds **6a** and **6b**. The intersection of a row column gives the CP3 score and the corresponding probability, for a pair of diastereoisomers, that one of these matches compound **6a** and the other, compound **6b**.

	6a goes with:			
	(10*R*-10′*S*)-*gauche* 1		(10*R*-10′*S*)-*gauche* 2	
6b goes with:	CP3	P	CP3	P
(10*R*,10′*R*)-*gauche* 1	−0.19	2	−0.58	0
(10*R*,10′*R*)-*gauche* 2	0.81	100	0.73	100

trifluoroacetic acid-water). TLC was performed on pre-coated silica gel aluminum sheets (Kieselgel 60 F254, 0.20 mm, Merck). The plates were visualized under UV light (254 and 365 nm) and using anisaldehyde-H_2SO_4 reagent. Preparative TLC was conducted on silica plates Macherey-Nagel SIL G-25 UV254 (20 × 20 cm, 0.25 mm). Chromatographic separation was performed using C18-functionalized silica gel (LiChroprep® 15–25 μm, Merck). MPLC was carried out using the Büchi pump model C-605, C-615. Acetone, ethyl acetate, dichloromethane, toluene (all with purity ≥99.8%), and orthophosphoric acid (85%) were purchased from Carlo Erba. Methanol (HPLC grade, ≥ 99.8%), chloroform (≥99.2%), and formic acid (≥99.3%) from VWR International.

4.2. Lichen material

Nephroma laevigatum samples were collected in Soudeilles (France; 45°26′N. 2°2′E) on October 2014. This species grows on bark in humid mossy communities of markedly oceanic old-growth forests and is quite sensitive to pollutants. The upper surface is grey-brown and apothecia are scabrid-areolate, ridged and frequent. Samples were identified by thalline chemical tests and stored in the herbarium at the Faculté de Pharmacie, Université de Limoges, France (HL-L1014-01). The identification was checked by lichenologists from the AFL (French Association of Lichenology).

4.3. Extraction and isolation

A sample of cleaned and dried lichen (50 g) was extracted by CH_2Cl_2 (5 L) at room temperature under agitation. After concentration, a red-brown extract (2.9 g) was obtained. The extract was chromatographed on silica gel chromatography using a gradient of C_6H_{12}/EtOAc 95:5 to EtOAc followed by a mixture of MeOH/EtOAc 50:50. Fractions were collected and analyzed by TLC and grouped following their chemical composition. Thus, 15 fractions (F1 to F15) were obtained.

The fraction F7 (116.0 mg) was purified by a reversed phase chromatography to give fraction F7c (30.0 mg). This subfraction was submitted to a silica gel MPLC eluted with C_6H_{12}/EtOAc 80:20 to obtain 10 mg of compound **1**.

The fraction F11 (0,830 g) was subjected to a second purification on 40 g of Sephadex® LH-20 eluted with $CHCl_3$/MeOH (90:10 to 0:100) to provide 11 fractions (F11a to F11k). Purification of F11a (208 mg) by preparative TLC give the compound **3** (15 mg) and **4** (26 mg). Purification of F11b (214 mg) by semi-preparative HPLC generates the compound **2** (3 mg). Purification of fraction F11c (60.0 mg) yields the compounds **2** (30 mg), **5a** (7.4 mg), **5b** (9.0 mg) and **6a** (9.5 mg) and **6b** (14.3 mg).

(±)-Nephrolaevigatin A or 7-chloroemodine bianthrone (**5a**): Yellowish powder; $[\alpha]^{20}_D$ + 5 (*c* 0.002, $(Me)_2CO$); ^1H and ^{13}C NMR (in DMSO-d_6), see Table 1; R_t 24.016 min; HRESIMS negative *m/z* 577.0488 $[M\text{-}H]^-$ (calcd for $C_{30}H_{19}O_8Cl_2$ 577.04515). The MS/MS spectrum was deposited in the GNPS spectral library under the identifier: CCMSLIB00005724340.

(±)-Nephrolaevigatin B or 7-chloroemodine bianthrone (**5b**): Yellowish powder; $[\alpha]^{20}_D$ + 9 (*c* 0.002, $(Me)_2CO$); ^1H and ^{13}C NMR (in DMSO-d_6), see Table 1; R_t 25.667 min; HRESIMS negative *m/z* 577.0488 [M-H]- (calcd for $C_{30}H_{19}O_8Cl_2$ 577.04515). The MS/MS spectrum was deposited in the GNPS spectral library under the identifier: CCMSLIB00005724341.

(+)-Nephrolaevigatin C or (+)-(10*R**, 10′*S**) emodine–7-chloroemodine bianthrone (**6a**): Yellowish powder; $[\alpha]^{20}_D$ + 66 (*c* 0.01, MeCN); ^1H and ^{13}C NMR (in DMSO-d_6), see Table 1; R_t 21.471 min; HRESIMS negative *m/z* 543.0866 $[M\text{-}H]^-$ (calcd for $C_{30}H_{20}O_8Cl$ 543.08412). The MS/MS spectrum was deposited in the GNPS spectral library under the identifier: CCMSLIB00005724339.

(±)-Nephrolaevigatin D or (±)-(10*R**, 10′*R**) emodine – 7-chloroemodine bianthrone (**6b**): Yellowish powder; $[\alpha]^{20}_D$ 0 (*c* 0.002, $(Me)_2CO$); ^1H and ^{13}C NMR (in DMSO-d_6), see Table 1; R_t 18.34 min; HRESIMS negative *m/z* 543.0866 $[M\text{-}H]^-$ (calcd for $C_{30}H_{20}O_8Cl$ 543.08412). The MS/MS spectrum was deposited in the GNPS spectral library under the identifier: CCMSLIB00005724338.

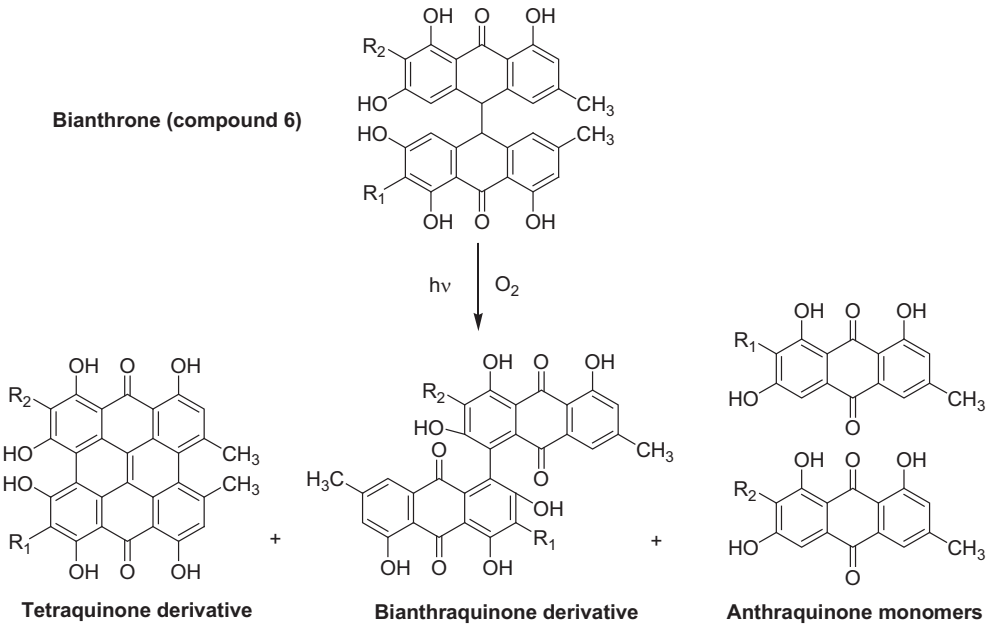

Fig. 3. Degradation products of bianthrones in presence of light and oxygen.

4.4. Data dependent LC-ESI-HRMS^2 analysis

LC-ESI-HRMS^2 analyses were achieved by coupling the LC system to a hybrid quadrupole time of-flight mass spectrometer Agilent 6530 (Agilent Technologies, Massy, France) equipped with an ESI source, operating in positive-ion mode. Source parameters were set as followed: capillary temperature at 320 °C, source voltage at 3500 V, sheath gas flow rate at 10 L.min^{-1}. The divert valve was set to waste for the first 3 min. MS scans were operated in full-scan mode from *m/z* 100 to 1700 (0.1 s scan time) with a mass resolution of 11,000 at *m/z* 922. MS1 scan was followed by MS2 scans of the five most intense ions above an absolute threshold of 5000 counts. Selected parent ions were fragmented at a collision energy fixed at 45 eV and an isolation window of 1.3 amu. Calibration solution, containing two internal reference masses (purine, $C_5H_4N_4$, *m/z* 121.050873, and HP-921 [hexakis-(1H,1H,3H-tetrafluoropentoxy)phosphazene], $C_{18}H_{18}O_6N_3P_3F_{24}$, *m/z* 922.0098). A permanent MS/MS exclusion list criterion was set to prevent oversampling of the internal calibrant. LC-UV and MS data acquisition and processing were performed using MassHunter Workstation software (Agilent Technologies, Massy, France).

4.5. Feature-based molecular networking

The MS^2 data files, related to the dichloromethane extract of *Nephroma laevigatum* were converted from the .d (Agilent) standard data-format to .mzXML format using the MSConvert software, part of the ProteoWizard package [37]. All .mzXML were then processed using MZmine 2 v52 [38]. The mass detection was realized keeping the noise level at 1.2E3 at MS1 and at 2E1 at MS2. The ADAP chromatogram builder was used using a minimum group size of scans of 2, a group intensity threshold of 2E3, a minimum highest intensity of 2E3 and *m/z* tolerance of 10 ppm [39]. The chromatogram deconvolution was performed using the Local Minimum Search algorithm with the following settings: chromatographic threshold = 1%, search minimum in RT range (min) = 0.1, minimum relative height = 5%, minimum absolute height = 2E3, min ratio of peak top/edge = 1.4, peak duration range (min) = 0.05–2. MS2 scans were paired using a *m/z* tolerance range of 0.02 Da and RT tolerance range of 1.5 min. Isotopes were grouped using the isotopic peaks grouper algorithm with a *m/z* tolerance of 10 ppm and a RT tolerance of 1.3 min with the most intense peak. The adduct search module was used repeatedly to perform the annotation of the chlorination pattern [40] using the following parameters (in this order): for Cl_2, mass_difference = −1.997, Max relative adduct peak height < 180%; for Cl, mass_difference = −1.997, Max relative adduct peak height < 400%, RT tolerance = 1.3 min, *m/z* tolerance = 10 ppm. The resulted peak list was filtered to keep only rows with MS2 features. The .mgf file was exported using the dedicated "Export/Submit to GNPS/FBMN" option. The .csv file (for RT, areas and identities regarding the chlorination patterns) was generated separately. The raw data files related to the LC-MS/MS analysis were deposited on the public MassIVE repository under the accession number: MSV000086130.

4.6. Molecular networking parameters

A molecular network was created using the online FBMN workflow (version release_20) at GNPS (http://gnps.ucsd.edu) with a parent mass tolerance of 0.02 Da and an MS/MS fragment ion tolerance of 0.02 Da. A network was then created where edges were filtered to have a cosine score above 0.65 and more than 6 matched peaks. Further edges between two nodes were kept in the network if and only if each of the nodes appeared in each other's respective top 10 most similar nodes. The spectra in the network were then searched against GNPS spectral libraries. All matches kept between network spectra and library spectra were required to have a score above 0.65 and at least 6 matched peaks. The molecular networking data were analyzed and visualized using Cytoscape (ver. 3.6.0) [41].

4.7. Computational details for GIAO NMR chemical shifts calculations

All DFT calculations were performed using the Gaussian 09.A01 program [42]. The calculations of the NMR spectra consisted in three successive steps. For each compound **5** and **6**, isomers C-10 R/C-10′ R and C-10 R/C-10′ S were first subjected to a conformational search using the MMFF94 force-field implemented in TINKER software tools. The resulting lowest energy conformations were then subjected to further optimization at the MPW1PW91/6–31 + G(d,p) level of theory. The bulk solvent effects were described with the integral equation formalism polarizable continuum Model (IEFPCM) with DMSO as solvent [43]. Vibrational frequencies were computed using the gauge-including atomic orbitals (GIAO) [44,45] method with the same level theory.

The resulting shielding tensors were averaged using the Boltzmann distribution. The chemical shifts were calculated from TMS as reference standard. The systematic errors were removed by scaling according to $\delta_{scaled} = (\delta_{calc} - Intercept)/Slope$, where *Intercept* and *Slope*, result from a linear regression calculation on a plot of δ_{calc} against δ_{exp} [44]. The CP3 probabilities were then computed as originally described by Smith and Goodman [25].

Declaration of Competing Interest

The authors declare that there is no conflict of interest for the financial support and the redaction of the manuscript. All the authors listed have approved the above manuscript. I declare on behalf of my co-authors that this work has not been published previously elsewhere in whole or in part.

Acknowledgements

This work was supported by Limousin Region (doctorale fellowship grant for A. Lagarde). This work was also financially supported by the ANR (Agence Nationale de la Rencherche, France) (ANR-17-CE35-0005). We are also grateful to A-L. Rioux, M. Arfeuillère for technical assistance and to Mrs. E. Pinault for HR-MS analysis.

Appendix A. Supplementary data

Electronic supplementary information file (ESI) is available for this manuscript. This additional file contains NMR spectra of compound **5–6**, the global networking of the dichloromethane extract and additional figures.

References

[1] C.W. Smith, A. Aptroot, B.J. Coppins, A. Fletcher, O.L. Gilbert, J. Wolseley, P. A. Wolseley, The lichens of Great Britain and Ireland, British Lichen Soc. (2009) 1–1046.

[2] G. Bendz, G. Bohman, J. Santesson, Chlorinated Anthraquinones from *Nephroma laevigatum*, Acta Chem. Scand. 21 (1967) 2889–2890.

[3] P.A. Cohen, G.H.N. Towers, Anthraquinones and phenanthroperylenequinones from *Nephroma laevigatum*, J. Nat. Prod. 58 (1995) 520–526, https://doi.org/10.1021/np50118a006.

[4] A. Wilkins, Nephrin: structure and occurence in *Nephroma* species, Phytochemistry. 19 (1980) 696–697.

[5] C. Roullier, M. Chollet-Krugler, E.-M. Pferschy-Wenzig, A. Maillard, G. N. Rechberger, B. Legouin-Gargadennec, R. Bauer, J. Boustie, Characterization and identification of mycosporines-like compounds in cyanolichens. Isolation of mycosporine hydroxyglutamicol from *Nephroma laevigatum* Ach, Phytochemistry. 72 (2011) 1348–1357, https://doi.org/10.1016/j.phytochem.2011.04.002.

[6] A. Lagarde, M. Millot, A. Pinon, B. Liagre, M. Girardot, C. Imbert, T.S. Ouk, P. Jargeat, L. Mambu, Antiproliferative and antibiofilm potentials of endolichenic fungi associated with the lichen *Nephroma laevigatum*, J. Appl. Microbiol. 126 (2019) 1044–1058, https://doi.org/10.1111/jam.14188.

[7] L.P. Mai, F. Guéritte, V. Dumontet, M.V. Tri, B. Hill, O. Thoison, D. Guénard, T. Sévenet, Cytotoxicity of Rhamnosylanthraquinones and Rhamnosylanthrones from *Rhamnus nepalensis*, J. Nat. Prod. 64 (2001) 1162–1168, https://doi.org/10.1021/np010030v.

[8] L. Du, T. Zhu, H. Liu, Y. Fang, W. Zhu, Q. Gu, Cytotoxic polyketides from a marine-derived fungus *Aspergillus glaucus*, J. Nat. Prod. 71 (2008) 1837–1842, https://doi.org/10.1021/np800303t.

[9] B.N. Lenta, K.P. Devkota, S. Ngouela, F.F. Boyom, Q. Naz, M.I. Choudhary, E. Tsamo, P.J. Rosenthal, N. Sewald, Anti-plasmodial and cholinesterase inhibiting activities of some constituents of *Psorospermum glaberrimum*, Chem. Pharm. Bull. (Tokyo) 56 (2008) 222–226.

[10] Y. Zheng, G. Yin, V. Le, A. Zhang, Y. Lu, M. Yang, Z. Fei, J. Liu, Hypericin-based photodynamic therapy induces a tumor-specific immune response and an effective DC-based cancer immunotherapy, Biochem. Pharmacol. (2014), https://doi.org/10.1016/j.bcp.2014.01.036.

[11] Z. Machatová, Z. Barbieriková, P. Poliak, V. Jančovičová, V. Lukeš, V. Brezová, Study of natural anthraquinone colorants by EPR and UV/Vis spectroscopy, Dyes Pigments 132 (2016) 79–93, https://doi.org/10.1016/j.dyepig.2016.04.046.

[12] J. Lemli, R. Dequeker, J. Cuveele, The palmidins, a new group of dianhrones from the fresh roots of *Rheum palmatum*, Planta Med. 12 (1964) 107–111.

[13] L.-F. Nothias, D. Petras, R. Schmid, K. Dührkop, J. Rainer, A. Sarvepalli, I. Protsyuk, M. Ernst, H. Tsugawa, M. Fleischauer, F. Aicheler, A.A. Aksenov, O. Alka, P.-M. Allard, A. Barsch, X. Cachet, A.M. Caraballo-Rodriguez, R.R. Da Silva, T. Dang, N. Garg, J.M. Gauglitz, A. Gurevich, G. Isaac, A.K. Jarmusch, Z. Kameník, K.B. Kang, N. Kessler, I. Koester, A. Korf, A. Le Gouellec, M. Ludwig, C. Martin, H.L.-I. McCall, J. McSayles, S.W. Meyer, H. Mohimani, M. Morsy, O. Moyne, S. Neumann, H. Neuweger, N.H. Nguyen, M. Nothias-Esposito, J. Paolini, V. Phelan, T. Pluskal, R.A. Quinn, S. Rogers, B. Shrestha, A. Tripathi, J.J. J. van der Hooft, F. Vargas, K.C. Weldon, M. Witting, H. Yang, Z. Zhang, F. Zubeil, O. Kohlbacher, S. Böcker, T. Alexandrov, N. Bandeira, M. Wang, P.C. Dorrestein, Feature-based molecular networking in the GNPS analysis environment, Nat. Methods 17 (2020) 905–908, https://doi.org/10.1038/s41592-020-0933-6.

[14] D. Olivier-Jimenez, M. Chollet-Krugler, D. Rondeau, M.A. Beniddir, S. Ferron, T. Delhaye, P.-M. Allard, J.-L. Wolfender, H.J.M. Sipman, R. Lücking, J. Boustie, P. Le Pogam, A database of high-resolution MS/MS spectra for lichen metabolites, Sci. Data. 6 (2019), https://doi.org/10.1038/s41597-019-0305-1.

[15] M. Wang, J.J. Carver, V.V. Phelan, L.M. Sanchez, N. Garg, Y. Peng, D.D. Nguyen, J. Watrous, C.A. Kapono, T. Luzzatto-Knaan, C. Porto, A. Bouslimani, A.V. Melnik, M.J. Meehan, W.-T. Liu, M. Crüsemann, P.D. Boudreau, E. Esquenazi, M. Sandoval-Calderón, R.D. Kersten, L.A. Pace, R.A. Quinn, K.R. Duncan, C.-C. Hsu, D.J. Floros, R.G. Gavilan, K. Kleigrewe, T. Northen, R.J. Dutton, D. Parrot, E.E. Carlson, B. Aigle, C.F. Michelsen, L. Jelsbak, C. Sohlenkamp, P. Pevzner, A. Edlund, J. McLean, J. Piel, B.T. Murphy, L. Gerwick, C.-C. Liaw, Y.-L. Yang, H.-U. Humpf, M. Maansson, R.A. Keyzers, A.C. Sims, A.R. Johnson, A.M. Sidebottom, B.E. Sedio, A. Klitgaard, C.B. Larson, C.A. Boya, P.D. Torres-Mendoza, D.J. Gonzalez, D. B. Silva, L.M. Marques, D.P. Demarque, E. Pociute, E.C. O'Neill, E. Briand, E.J. N. Helfrich, E.A. Granatosky, E. Glukhov, F. Ryffel, H. Houson, H. Mohimani, J. J. Kharbush, Y. Zeng, J.A. Vorholt, K.L. Kurita, P. Charusanti, K.L. McPhail, K. F. Nielsen, L. Vuong, M. Elfeki, M.F. Traxler, N. Engene, N. Koyama, O.B. Vining, R. Baric, R.R. Silva, S.J. Mascuch, S. Tomasi, S. Jenkins, V. Macherla, T. Hoffman, V. Agarwal, P.G. Williams, J. Dai, R. Neupane, J. Gurr, A.M.C. Rodríguez, A. Lamsa, C. Zhang, K. Dorrestein, B.M. Duggan, J. Almaliti, P.-M. Allard, P. Phapale, L.-F. Nothias, T. Alexandrov, M. Litaudon, J.-L. Wolfender, J.E. Kyle, T. O. Metz, T. Peryea, D.-T. Nguyen, D. VanLeer, P. Shinn, A. Jadhav, R. Müller, K. M. Waters, W. Shi, X. Liu, L. Zhang, R. Knight, P.R. Jensen, B.Ø. Palsson, K. Pogliano, R.G. Linington, M. Gutiérrez, N.P. Lopes, W.H. Gerwick, B.S. Moore, P. C. Dorrestein, N. Bandeira, Sharing and community curation of mass spectrometry data with Global Natural Products Social Molecular Networking, Nat. Biotechnol. 34 (2016) 828–837, https://doi.org/10.1038/nbt.3597.

[16] A.E. Fox Ramos, L. Evanno, E. Poupon, P. Champy, M.A. Beniddir, Natural products targeting strategies involving molecular networking: different manners, one goal, Nat. Prod. Rep. 36 (2019) 960–980, https://doi.org/10.1039/C9NP00006B.

[17] A.E. Fox Ramos, C. Pavesi, M. Litaudon, V. Dumontet, E. Poupon, P. Champy, G. Genta-Jouve, M.A. Beniddir, CANPA: computer-assisted natural products anticipation, Anal. Chem. 91 (2019) 11247–11252, https://doi.org/10.1021/acs.analchem.9b02216.

[18] S. Duperron, M.A. Beniddir, S. Durand, A. Longeon, C. Duval, O. Gros, C. Bernard, M.-L. Bourguet-Kondracki, New benthic cyanobacteria from Guadeloupe mangroves as producers of antimicrobials, Mar. Drugs. 18 (2019) 16, https://doi.org/10.3390/md18010016.

[19] G. Cauchie, E.O. N'Nang, J.J.J. van der Hooft, P. Le Pogam, G. Bernadat, J.-F. Gallard, B. Kumulungui, P. Champy, E. Poupon, M.A. Beniddir, Phenylpropane as an alternative Dearomatizing unit of Indoles: discovery of Inaequalisines a and B using substructure-informed molecular networking, Org. Lett. 22 (2020) 6077–6081, https://doi.org/10.1021/acs.orglett.0c02153.

[20] I. Yosioka, H. Yamauchi, K. Morimoto, I. Kitagawa, Three new chlorine containing bisanthronyls from a lichen, *Anaptychia obscurata* Vain, Tetrahedron Lett. 34 (1968) 3749–3752.

[21] P.A. Cohen, G.N. Towers, The anthraquinones of *Heterodermia obscurata*, Phytochemistry. 40 (1995) 911–915.

[22] I.C. Form, M. Bonus, H. Gohlke, W. Lin, G. Daletos, P. Proksch, Xanthone, benzophenone and bianthrone derivatives from the hypersaline lake-derived fungus *Aspergillus wentii*, Bioorg. Med. Chem. 27 (2019) 115005, https://doi.org/10.1016/j.bmc.2019.07.021.

[23] N.-Y. Ji, X.-R. Liang, R.-R. Sun, F.-P. Miao, A rule to distinguish diastereomeric bianthrones by 1H NMR, RSC Adv. 4 (2014) 7710, https://doi.org/10.1039/c3ra47055e.

[24] A.H. Aly, A. Debbab, C. Clements, R. Edrada-Ebel, B. Orlikova, M. Diederich, V. Wray, W. Lin, P. Proksch, NF kappa B inhibitors and antitrypanosomal metabolites from endophytic fungus *Penicillium* sp. isolated from *Limonium tubiflorum*, Bioorg. Med. Chem. 19 (2011) 414–421, https://doi.org/10.1016/j.bmc.2010.11.012.

[25] S.G. Smith, J.M. Goodman, Assigning the stereochemistry of pairs of Diastereoisomers using GIAO NMR shift calculation, J. Org. Chem. 74 (2009) 4597–4607, https://doi.org/10.1021/jo900408d.

[26] H. Meyer, Über neue Reduktionsprodukte des Anthrachinons, Ber. Dtsch. Chem. Ges. 42 (1909) 143–145, https://doi.org/10.1002/cber.19090420118.

[27] A.V. El'tsov, Organic Photochromes, Springer US, Boston, MA, 1990. http://public.eblib.com/choice/publicfullrecord.aspx?p=3083107 (accessed February 27, 2019).

[28] R.D.L. Johnstone, D. Allan, A. Lennie, E. Pidcock, R. Valiente, F. Rodríguez, J. Gonzalez, J. Warren, S. Parsons, The effect of pressure on the crystal structure of bianthrone, Acta Crystallogr. B 67 (2011) 226–237, https://doi.org/10.1107/S0108768111009657.

[29] S. Mattar, D. Sutherland, Oxidation-reduction behavior of bianthrone and bianthronyl in basic dimethylsulfoxide solutions, J. Phys. Chem. 95 (1991) 5129–5133.

[30] D. Cameron, J.S. Edmonds, W.D. Raverty, Oxidation of emodin anthrone and stereochemistry of emodin bianthrone, Aust. J. Chem. 29 (1976) 1535–1548.

[31] J. Bruneton, E. Poupon, Pharmacognosie, Phytochimie, Plantes Médicinales, Tec & Doc, Paris, 2016.
[32] P. Cohen, N. Towers, Biosynthetic studies on chlorinated anthraquinones in the lichen *Nephroma laevigatum*, Phytochemistry. 42 (1996) 1325–1329.
[33] U. Søchting, P. Frödén, Chemosyndromes in the lichen genus Teloschistes (Teloschistaceae, Lecanorales), Mycol. Prog. 1 (2002) 257–266.
[34] M. Giralt, G. Paz-Bermúdez, J.A. Elix, New data on *Sculptolumina japonica* (Physciaceae), Bryologist 112 (2009) 397–403, https://doi.org/10.1639/0007-2745-112.2.397.
[35] P.E. Mandelare, D.A. Adpressa, E.N. Kaweesa, L.N. Zakharov, S. Loesgen, Coculture of two developmental stages of a marine-derived *Aspergillus alliaceus* results in the production of the cytotoxic bianthrone Allianthrone A, J. Nat. Prod. 81 (2018) 1014–1022, https://doi.org/10.1021/acs.jnatprod.8b00024.
[36] G.A. Kemegne, P. Mkounga, J.J. Essia Ngang, S.L. Sado Kamdem, A.E. Nkengfack, Antimicrobial structure activity relationship of five anthraquinones of emodine type isolated from *Vismia laurentii*, BMC Microbiol. 17 (2017), https://doi.org/10.1186/s12866-017-0954-1.
[37] M.C. Chambers, B. Maclean, R. Burke, D. Amodei, D.L. Ruderman, S. Neumann, L. Gatto, B. Fischer, B. Pratt, J. Egertson, K. Hoff, D. Kessner, N. Tasman, N. Shulman, B. Frewen, T.A. Baker, M.-Y. Brusniak, C. Paulse, D. Creasy, L. Flashner, K. Kani, C. Moulding, S.L. Seymour, L.M. Nuwaysir, B. Lefebvre, F. Kuhlmann, J. Roark, P. Rainer, S. Detlev, T. Hemenway, A. Huhmer, J. Langridge, B. Connolly, T. Chadick, K. Holly, J. Eckels, E.W. Deutsch, R. L. Moritz, J.E. Katz, D.B. Agus, M. MacCoss, D.L. Tabb, P. Mallick, A cross-platform toolkit for mass spectrometry and proteomics, Nat. Biotechnol. 30 (2012) 918–920, https://doi.org/10.1038/nbt.2377.
[38] T. Pluskal, S. Castillo, A. Villar-Briones, M. Oresic, MZmine 2: modular framework for processing, visualizing, and analyzing mass spectrometry-based molecular profile data, BMC Bioinform. 11 (2010) 1–11, https://doi.org/10.1186/1471-2105-11-395.
[39] O.D. Myers, S.J. Sumner, S. Li, S. Barnes, X. Du, One step forward for reducing false positive and false negative compound identifications from mass spectrometry metabolomics data: new algorithms for constructing extracted ion chromatograms and detecting chromatographic peaks, Anal. Chem. 89 (2017) 8696–8703, https://doi.org/10.1021/acs.analchem.7b00947.
[40] K.M. McManus, R.D. Kirk, C.W. Via, J.S. Lotti, A.F. Roduit, R. Teta, S. Scarpato, A. Mangoni, M.J. Bertin, Isolation of Isotrichophycin C and Trichophycins G–I from a collection of *Trichodesmium thiebautii*, J. Nat. Prod. (2020), https://doi.org/10.1021/acs.jnatprod.0c00550.
[41] P. Shannon, A. Markiel, O. Ozier, N.S. Baliga, J.T. Wang, D. Ramage, D. Amin, B. Schwikowski, T. Ideker, Cytoscape: a software environment for integrated models of biomolecular interaction networks, Genome Res. 13 (2003) 2498–2504, https://doi.org/10.1101/gr.1239303.
[42] M.J. Frisch, G.W. Trucks, H.B. Schlegel, G.E. Scuseria, M.A. Robb, J.R. Cheeseman, G. Scalmani, V. Barone, B. Mennuci, G.A. Petersson, H. Nakatsuji, M. Caricato, X. Li, H.P. Hratchian, A.F. Izmaylov, J. Bloino, G. Zheng, J.L. Sonnenberg, M. Hada, M. Ehara, K. Toyota, R. Fukuda, J. Hasegawa, M. Ishida, T. Nakajima, Y. Honda, O. Kitao, H. Nakai, T. Vreven, J.A. Montgomery, J.E. Peralta, F. Ogliaro, M. Bearpark, J.J. Heyd, E. Brothers, K.N. Kudin, V.N. Staroverov, T. Keith, R. Kobayashi, J. Normand, K. Raghavachari, A. Rendell, J.C. Burant, S.S. Iyengar, J. Tomasi, M. Cossi, N. Rega, J.M. Millam, M. Klene, J.E. Knox, J.B. Cross, V. Bakken, C. Adamo, J. Jaramillo, R. Gomperts, R.E. Stratmann, O. Yazyev, A. J. Austin, R. Cammi, C. Pomelli, J.W. Ochterski, R.L. Martin, K. Morokuma, V. G. Zakrzewski, G.A. Voth, P. Salvador, J.J. Dannenberg, S. Dapprich, A.D. Daniels, O. Farkas, J.B. Foresman, J.V. Ortiz, J. Cioslowski, D.J. Fox, Gaussian 09, Wallingford CT, 2013.
[43] J. Tomasi, B. Mennucci, R. Cammi, Quantum mechanical continuum solvation models, Chem. Rev. 105 (2005) 2999–3094, https://doi.org/10.1021/cr9904009.
[44] G. Barone, L. Gomez-Paloma, D. Duca, A. Silvestri, R. Riccio, G. Bifulco, Structure validation of natural products by quantum-mechanical GIAO calculations of 13C NMR chemical shifts GIAO=gauge including atomic orbitals, Chem. Eur. J. 8 (2002) 3233, https://doi.org/10.1002/1521-3765(20020715)8:14<3233::AID-CHEM3233>3.0.CO;2-0.
[45] G. Schreckenbach, T. Ziegler, Calculation of NMR shielding tensors using gauge-including atomic orbitals and modern density functional theory, J. Phys. Chem. 99 (1995) 606–611, https://doi.org/10.1021/j100002a024.